Electronic structure of metal phthalocyanines on Ag (100)

Cornelius Krull

Ph.D. Thesis

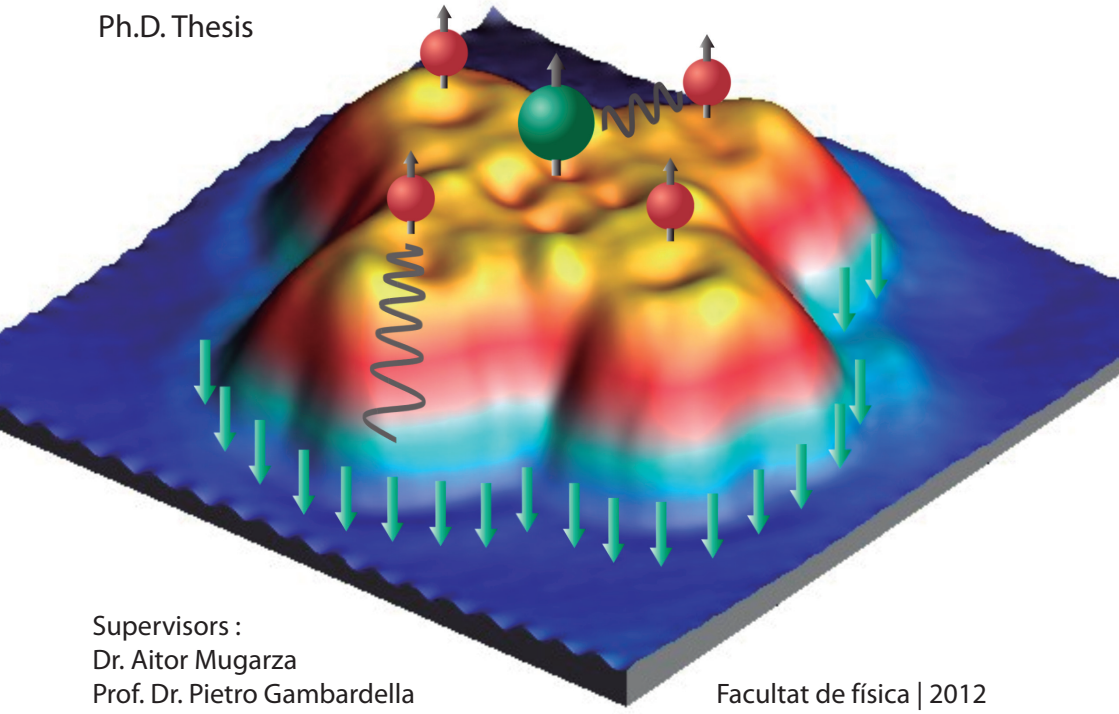

Supervisors :
Dr. Aitor Mugarza
Prof. Dr. Pietro Gambardella

Facultat de física | 2012

Institut Català de Nanotecnologia
Universitat Autònoma de Barcelona

Chapter 5

5 Electronic and magnetic properties of MePc on Ag(100)

For numerous technological applications it is necessary to place molecules on a supporting surface or an electrode. However many interesting physical properties of molecules are perturbed when adsorbed on a surface, complicating the reproducible design of hybrid molecular electronic devices. On a metal surface, the electronic interactions distort the ligand field [169], induce charge transfer processes [150, 170, 152], and reduce the d-d electron correlation at metal ions by screening and hybridization [170, 152]. The complex interplay between all these processes is far from being understood, as reflected by the intense research carried out on this topic during the last years.

Most studies of the magnetic properties of MePc have focused on MnPc [114, 150], FePc [170, 111, 133, 150], and CoPc [152, 150, 171, 170, 172, 173, 127, 146, 174]. A general tendency seems to be that the adsorption on a metallic surface reduces or quenches the magnetic moment of the TM ion. On the other hand, more systematic studies of different MePcs carried out by photoemission [151, 175] and Density Functional Theory (DFT) [150] show a strong influence of the spatial extension of TM-d states on the modification of electronic and magnetic properties at the interface. The perturbation is weakest when the d states near the Fermi level lie in the molecular plane.

Common to such investigations is the assumption that the magnetic

properties of MePc at surfaces depends almost exclusively on the ground state of the metal ion, while the ligand part is regarded mainly as a mediator controlling the environment of the magnetic atom. The case of CoPc on Au(111) is an example, where the appearance and disappearance of a Kondo resonance, i.e., the interaction of the magnetic ion with the substrate was mediated by chemically changing the organic ligand [110]. Later on in this chapter we will show that the ligand cannot be regarded only in such a manner, and that it can actively participate in the magnetism of the entire complex. Indeed, a growing number of experiments indicates that the organic ligand directly affects the magnetism and transport properties of metal-organic [99, 174, 176] as well as purely organic complexes [94] adsorbed on surfaces.

Other factors have an impact on the coupling between molecule and substrate as well. For instance, two different adsorption sites for FePc on Au(111) have been observed to lead to to different Kondo interactions [111]. The molecular coverage also plays a role. For coverages up to a monolayer, lateral molecule-molecule interactions increase, weakening the coupling to the substrate [129, 134]. In multilayers of MePc the lower layers can also vertically decouple the molecules, and the electronic structure evolves towards the semiconducting behavior of bulk MePcs.

In this chapter we will look at the electronic and magnetic structure of four different MePc (Me = Fe, Co, Ni, Cu) deposited on Ag(100), investigating the mechanisms that lead to changes in both the ion and ligand magnetic moments. Scanning tunneling spectroscopy (STS) combined with DFT calculations, performed by R. Robles and N. Lorente, allows us to explain the role of charge transfer, hybridization, and correlation on the electronic ground state and the magnetic properties.

We will start by reviewing the gas phase electronic structure to better contextualize the effects of the surface. The electronic structure of adsorbed MePc is discussed by comparing STS data with molecular projected density of states (PDOS) from ab-initio DFT. Afterwards the magnetic properties of MePc are addressed, using STS to measure the intensity and spatial extension of Kondo resonances in the differential conductance, including the coupling to vibrational and magnetic degrees of freedom. On the basis of these measurements combined with DFT results, we are able to propose a magnetic structure.

The end of the chapter will treat the effect of higher coverages on the electronic and magnetic properties, considering small clusters up mul-

tilayer structures. For clusters in the submonolayer regime we find a gradual change in the interaction with the substrate based on intermolecular interactions. In complete monolayers the relative strength of the different hybridization channels plays a critical role in determining the degree of decoupling through these interactions. Finally the multilayer system shows a complete decoupling from the substrate exhibiting typical effects for molecules in a double barrier junction.

5.1. Pristine MePc - gas phase electronic structure

It is useful to review the gas phase electronic structure of MePc, in order to better understand the effect of the substrate (see Figure 5.1).

MePcs are metal organic complexes, consisting of an organic ligand (Pc) and a transition metal atom (TM) in the center of 4 pyrole N (see Figure 4.1 on page 57). For most TM the bonding to the ligand has an ionic character and the ion is in a $[TM]^{2+}$ state. The molecule has a square planar D_{4h} symmetry. Under this ligand field symmetry, the TM's d states transform as b_{2g} (d_{xy}), b_{1g} ($d_{x^2-y^2}$), a_{1g} (d_{z^2}), and e_g ($d_{xz}/d_{yz} = d_\pi$). Depending on the overlap and energy position, they mix in different degree with the $2p$ states of neighboring C and N atoms. The TM-related d states will be classified in two groups according to their orientation with respect to the molecular/substrate plane: the parallel (b_{2g}, b_{1g} =d_{xy}, $d_{x^2-y^2}$= $d_{\shortparallel}$) or perpendicular (a_{1g}, e_g =d_{z^2}, d_{xz}, d_{yz}= $d_\perp$) states.

The gas phase HOMO/LUMO orbitals of the Pc ring are delocalized π orbitals with marginal TM-d contribution, represented respectively by $a_{1u}/2e_g$. The $2e_g$ (LUMO) is two fold degenerate, without considering the spin degree of freedom.

The TM centers used in this study are Fe, Co, Ni, Cu. All of them are 3d TM with increasing occupation of the d-level from Fe(d^6) to Cu(d^9). Figure 5.1 shows the the distribution of the energy levels near the Fermi level obtained with GGA+U, with U-J=3eV, the TM-d contribution in each MO is indicated. The resulting magnetic moments are also shown. The electronic structure of the Pc ring is barely affected by the type of TM ion. This is clearly seen for the a_{1u} and $2e_g$ ligand orbitals: The a_{1u} has a negligible d contribution and appears at the same energy for all molecules. The $2e_g$ energy varies slightly with the d configuration of the TM ion, and exhibits some intermixing with the d_π state occurs, ranging from 7% in FePc, to 1% in CuPc. The different degree of hybridization depends on the

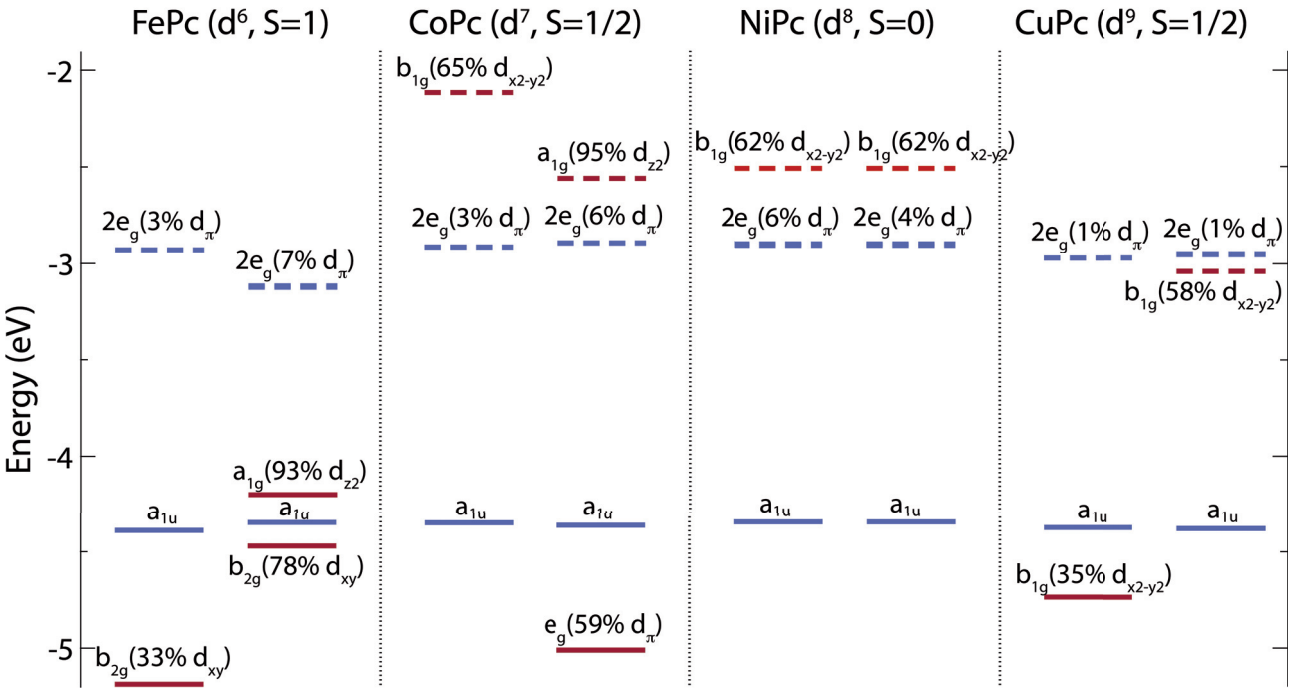

Figure 5.1.: Spin-polarized electronic structure of gas-phase MePc: The contribution of different d states is indicated in percentage. Blue lines indicate states that are largely localized on the Pc ligand part, while red lines represent states that originate mainly from the TM's d states. Note that $a_{1u}/2e_g$ refer to the gas phase HOMO/LUMO states of the Pc ring.

proximity of the two levels with e_g symmetry: the one with strong (e_g) and weak ($2e_g$) d_π contribution.
The evolution of the electronic configuration of the $[TM]^{2+}$ ions cannot be followed by a simple rigid filling of ligand field split levels, due to the strong d-d correlation and the energy-dependent hybridization with ligand states. This is especially true for the complex ground state of FePc. The different results obtained within each approximation reflect the discrepancies found in the literature [170, 177, 178, 179]. The discussion of these differences is beyond the scope of this work. However, independent of the method used, the total magnetic moment obtained for FePc is always S=1, which is in good agreement with previous studies [170, 177, 180, 179]. CoPc, with one electron more, presents a S=1/2 ($^2A_{1g}$) ground state with a single a_{1g} (d_{z^2}) hole. NiPc, with d^8, is in a closed-shell S=0 ($^1A_{1g}$) configuration. And lastly the CuPc molecule, with the d^9 Cu ion, has a single hole in the b_{1g} ($d_{x^2-y^2}$) state, resulting in a doublet (S=1/2) ground state ($^2B_{1g}$).

It is important to point out that in the two S=1/2 systems, namely CoPc and CuPc, the spin resides in orbitals with very different spatial distribution, i.e., $d_\perp$ and $d_{||}$ respectively. This will lead to a very different behavior in the interaction with the substrate, as shown in the following sections.

5.2. Single molecules: electronic structure

In this section we present the spectroscopic data of the molecules adsorbed on the Ag(100) surface. The energy of the MOs and other interface-related features is obtained from averaged dI/dV spectra, whereas spatial constant current maps of the dI/dV intensity at specific energies reveals their symmetry and distribution within the molecule. Experimental results are then compared to the density of states projected onto different MOs, which allows the identification of the orbital belonging to the observed peaks, and gives insight into the different processes occurring at the metallic interface.

5.2.1. Spectroscopy of molecular orbitals

A series of dI/dV spectra acquired in the energy range of the frontier MOs is displayed in Figure 5.2a. The a_{1u} and $2e_g$ orbitals of the Pc ring (the

gas phase HOMO/LUMO) can be easily identified by studying the spatial distribution of the peaks of the spectra acquired on the benzene (blue), presented as dI/dV maps in Figure 5.3. The appearance is similar to that found in other substrates [173], except for the chiral imprint discussed in the previous chapter. The energy position of the a_{1u} orbital is similar in all MePcs, continuously varying from -1.14 V in CoPc to -1.40 V in CuPc (unfortunately FePc was not explored with this energy range).

On the other hand, the spectral distribution of the $2e_g$ critically depends on the TM ion: In FePc and CoPc, a single unoccupied peak is observed at +0.39 V and +0.47 V respectively, whereas CuPc and NiPc exhibit two peaks around the Fermi level, at -0.29/+0.35 V and -0.35/+0.35 V respectively. Both peaks, however, can be associated with the $2e_g$ due to their similar spatial distribution. The localization of the lower energy peak below E_F indicates that the orbital is partially occupied, meaning a charge transfer from the substrate to the ligand $2e_g$ orbital.

The energy splitting of $\sim 0.65 - 0.70$ eV is within the range of the Coulomb repulsion energies obtained for π-orbitals in aromatic complexes of similar size [94, 181, 182]. We therefore assign the peaks to the single and double occupation of the $2e_g$ state.

The sharp peak appearing between the two $2e_g$ peaks is the Kondo resonance (see chapter 3) will be discussed in section 5.3. In CoPc and FePc the $2e_g$ remains unoccupied. Note that here a double peak structure is not seen, because of the short electron lifetime in molecules strongly coupled to metals, which prevents the double occupation of empty orbitals by tunneling electrons.

The MOs with d character can be tracked in the spectra taken at the TM ion (red in Figure 5.2a). The broad peak shifting downwards with increasing d state occupation from FePc (-0.4V) to NiPc (-1.5V) is due to the $d_\perp$ states, which are easy to observe in STS because of their strong coupling to the tip.In CuPc, these states lie below the probed energy range. The localization of this peak on the TM ion is confirmed by the dI/dV map of CoPc at -510 mV in Figure 5.3b.
In CoPc, the $d_\perp$ resonance appears well below E_F, suggesting the complete filling of the a_{1g} (d_{z^2}) orbital, and hence a switch in the charge transfer channel from the ligand $2e_g$ to TM-d states. In FePc, the tail of the $d_\perp$ peak crosses E_F, suggesting that these states are not fully occupied, similarly to FePc on Au(111) [170]. As we we will see in the next section this interaction will induce a complex reorganization of charge

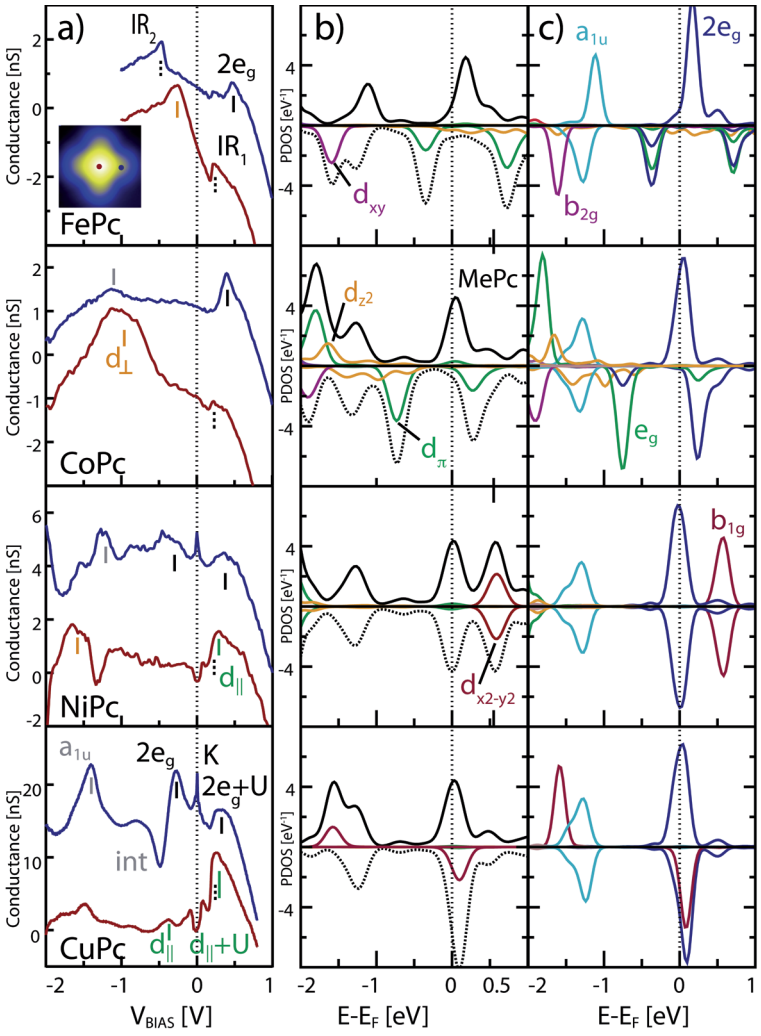

Figure 5.2.: a) dI/dV spectra, acquired on the metal ion (red) and the benzene ring (blue). The latter is shifted for clarity. The labeled features correspond to the $2e_g$ (black), a_{1u} (grey), $d_\perp$ (orange), $d_{\shortparallel}$ (green), interface states (dotted) and interference effects (int). Tunneling conditions: 1 nA, -1.0 V (FePc, CoPc), 3 nA, -2.2 V (NiPc), 3 nA, -2.0 V (CuPc). b) Computed spin-polarized PDOS projected onto the TM d states and onto the sum of all molecular orbitals, obtained by GGA + vdW.

that involves mixing of $d_\perp$ and ligand orbitals.

We can thus conclude that the charge transfer channel changes depending on the TM. Molecules with frontier $d_\perp$ orbitals (FePc, CoPc) interact through them, however when the $d_\perp$ states lie far from the Fermi level (NiPc, CuPc) the interaction occurs through the ligand $2e_g$ MO, which accepts an electron from the substrate.

The $d_{||}$ states seem to remain unperturbed after adsorption. Although the orientation parallel to the molecular plane makes them difficult to explore by STM, some features in the spectra of NiPc and CuPc can be tentatively assigned to b_{1g} ($d_{x^2-y^2}$). In the pristine molecules, this orbital is singly occupied in CuPc and unoccupied in NiPc (see Figure 5.1). The unoccupied contribution is overlapped by a step-like feature that appears around +0.2 V in all molecules. However, the higher intensity in this energy range compared to CoPc and FePc hints at the presence of the state in both CuPc and NiPc. The singly occupied b_{1g} orbital in CuPc can be assigned to the small hump observed around -0.4 V, in the same range where the $2e_g$ resonance at the benzene spectra presents a pronounced valley (labeled as int). This valley, absent in NiPc at this energy, may be related to a Fano lineshape originated from a tunneling interference between the occupied b_{1g} and the $2e_g$, analogous to that occurring between resonant and direct channels [183, 184]. Indeed, the dip observed in NiPc at the lower energy side, where $d_\perp$ states overlap with a_{1u}, supports the presence of Fano peaks in these molecules.

Apart from the resonances that maintain the character of pristine MOs, new interface resonances originate from the strong hybridization with Ag electrons, as shown in the dI/dV maps of Figure 5.4. The step-like IR_1 feature at +0.2 V, common to all MePcs and only observed on Ag(100), could originate from hybridization with a surface state that is close in energy [185]. In FePc, we observe an additional feature (IR_2) below the $d_\perp$ state, which we identify with an interface state with intensity at the benzene rings, similar to that reported for CoPc on Au(111) [173].

5.2.2. DFT: electronic structure

To correlate the peaks observed in the dI/dV spectra with the molecular electronic structure, we rely on the calculated DOS projected onto the TM-d states and the MOs of the MePc (see Figure 5.2b and c). In general we find fair agreement between the experimental data and the calculated PDOS,

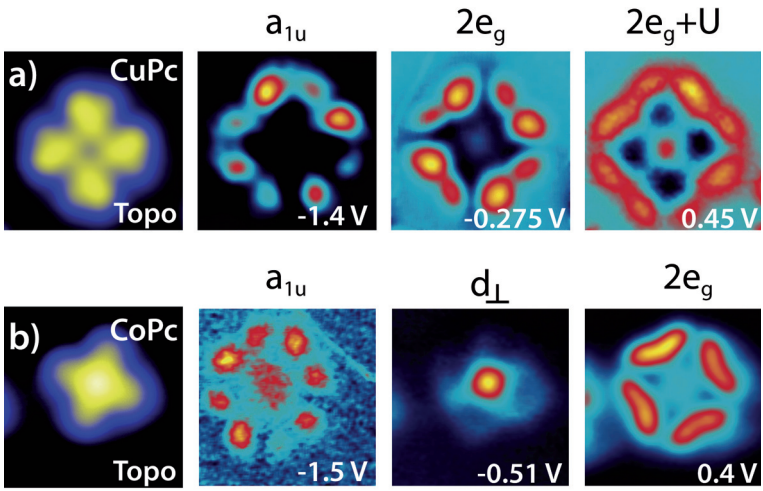

Figure 5.3.: Constant current dI/dV maps of CuPc a) and CoPc b), where the $d_\perp$ and ligand a_{1u} and $2e_g$ states can be identified. A topographic image obtained during the acquisition of maps is displayed on the left side. NiPc and FePc present similar MO distributions as CuPc and CoPc respectively.

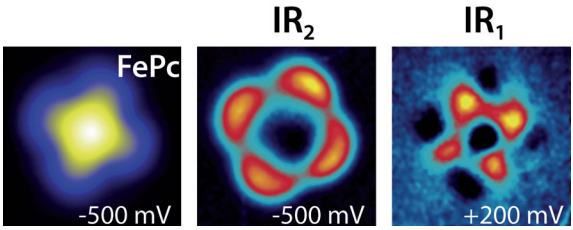

Figure 5.4.: Constant current dI/dV maps of interfacial states in FePc arising from the hybridization between molecular and substrate electrons (marked as IR_x in Figure 5.2b). A topographic image obtained during the acquisition of maps is displayed on the left side.

which allows us to assign many of the spectral feature to specific MO, based on the symmetry and spatial distribution of the dI/dV peaks.

The most hybridized states are the a_{1g} MOs of FePc and CoPc, as expected due to their dominant d_{z^2} character. The TM d_{z^2} -electrons hybridize with the Ag-sp_z states, confirming the strong, direct substrate-TM interaction discussed for the adsorption configuration in subsection 4.2.1

(page 57). Additionally, in the case of FePc and CoPc, two $2e_g$ and one e_g state are mixed together, projecting onto one occupied and one empty spin-down resonance (see Figure 5.2c). The mixing is induced by the hybridization with the substrate, showing that the picture of slightly distorted MO is no longer valid in this case. This is in line with the appearance of an interface resonance as observed in the STS maps (IR_2 in Figure 5.4).

For NiPc and CuPc, the hybridization with the substrate turns out to be much smaller, and the PDOS resembles that of the gas-phase molecules of Figure 5.1. In these two cases the confinement of the b_{1g} orbital in the molecular plane and its σ character reduce the intermixing with the Ag electrons, strongly decreasing the charge transfer to this orbital. Hence, it appears unoccupied in NiPc and singly occupied in CuPc, as in the gas-phase.

The a_{1u} orbital, fixed at about -1.30 eV, is the only MO that is not affected by the d-occupation of the TM ion. In the case of FePc, the spin up and spin down a_{1u} states are exchange-split due to the single-configurational nature of DFT. This broken symmetry reflects the strong spin-polarization of the whole molecule. The position of the $2e_g$ MO, on the other hand, depends on the type of TM ion and reveals a transition in the interaction with the substrate. As in the dI/dV spectra, the PDOS shows that this state is unoccupied in FePc, partially occupied in CoPc, and acquires a charge of approximately one electron in NiPc and CuPc. The splitting between occupied and unoccupied $2e_g$ states is not fully reproduced in the calculations due to the well-known electronic gap problem in DFT, which is especially critical for delocalized π-orbitals [186].

The dependence of the charge transfer behavior on the TM channel can be further understood by using gas-phase anions to study negatively charged MePc without any hybridization. We find that the TM-d dependent behavior is the same as in the adsorbates. In $[FePc]^{1-}$ and $[CoPc]^{1-}$ the effect of the extra electron is complex and the extra charge is not easily assigned to a single MO, it rather induces a reorganization of the charge within the molecule. In $[NiPc]^{1-}$ and $[CuPc]^{1-}$ the behavior is simpler, the $2e_g$ accepts the extra electron. This behavior is in agreement with transport results in electron-doped thin films [187].

5.3. Single molecules: magnetic structure

In the following we will focus on the analysis of the magnetic structure and its relation to the modified electronic properties studied in the previous section. Experimentally we use the Kondo interaction as an indirect way to probe the molecular spin with a non spin-polarized technique such as STS. For some molecules we observe a complex Kondo behavior, which can be explained through the use of DFT calculations, where the full magnetic structure of the molecules including the ligand and the ion is considered.

5.3.1. Kondo interaction

The Kondo interaction was introduced in chapter 3: it is the coupling of a localized impurity spin to a bath of underlying conduction electrons. Its main characteristic is that at temperatures below the characteristic Kondo energy $k_B T_K$ the localized spin is antiferromagnetically screened by the electrons in the Fermi sea, forming a many-body singlet ground state. The many body state appears as a sharp resonance at E_F, and is detectable by STM. Hence by taking dI/dV STS spectra around E_F on the molecules, we study their magnetic interaction with the substrate. In the most simple cases the molecular magnetic moment can be extracted from this data.

The dI/dV spectra obtained for the four cases are displayed in Figure 5.5. FePc and CoPc present featureless spectra, which indicate that the Kondo interaction between these molecules and the Ag(100) surface is either absent or too weak to be observed at 5 K.

Relatively flat Co spectra were reported also for CoPc adsorbed on Au(111), for which it was concluded that the filling of the a_{1g} state leads to a complete quenching of the molecular magnetic moment [172]. This interpretation has been recently questioned based on a mixed-valence model of x-ray absorption spectra [170]. In both cases, the quenching of the CoPc magnetic moment appears to be a robust result. On the other hand, FePc does present a Kondo resonance on Au(111), although different interaction strengths have been reported [111, 134]. We attribute the absence of Kondo peaks on Ag(100) to a stronger interaction with the substrate, as reflected by the substantial hybridization of the $d_\perp$ states, which may lead to a mixed-valence configuration of FePc, as discussed later.

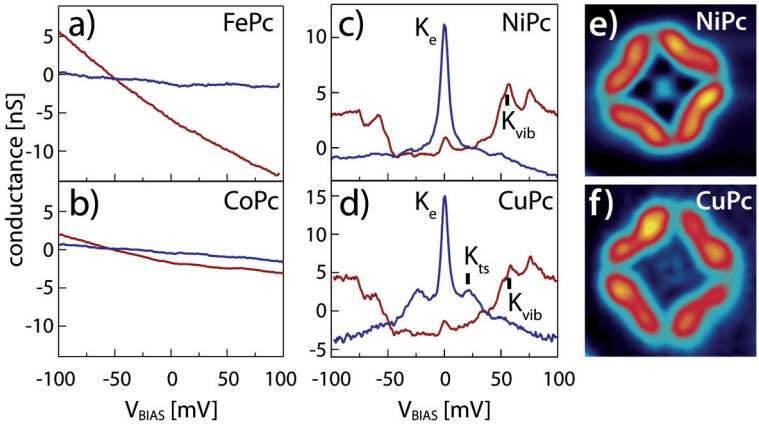

Figure 5.5.: a)-d) Conductance spectra acquired around E_F on the metal ion (red) and the benzene ring (blue). The zero-bias (elastic), vibrational, and triplet-singlet Kondo resonances observed in CuPc and NiPc are labelled as K_e, K_v and K_{ts} respectively. Tunneling conditions (I, V_b): 1 nA, -100 mV (FePc, CoPc), 1.1 nA, -100 mV (NiPc), 2 nA, -100 mV (CuPc). e) and f) d^2I/dV^2 map acquired at -3 mV and -5mV respectively, showing the intensity distribution of the elastic Kondo resonance (K_e) of CuPc and NiPc and its resemblance with the dI/dV map of the $2e_g$ orbital.

In contrast with FePc/CoPc the dI/dV spectra for NiPc and CuPc show many characteristic signatures of low-energy excitations. The most prominent peak, located at zero bias, is the elastic zero bias Kondo resonance K_e (see section 3.4.1 on page 47). The temperature dependence of its width and intensity are expected to follow expressions derived from Fermi liquid theory [88] and numerical renormalization group (NRG) [25]. We therefore recorded the STS at the benzene at different temperatures. In Figure 5.6 we display the results obtained for CuPc, confirming the Kondo behavior. Fitting the values of the width (Γ_K) with Equation 3.21 yields a Kondo temperature of T_K = 27 $\pm$ 2 K. The logarithmic behavior of the intensity (G_K) makes it more sensitive to the scattering of the data, but we can see that expressions for both S=1/2 and the underscreened S=1 fit reasonably well the data by using T_K = 27 K. Unfortunately the two cases diverge only at temperatures that are not experimentally accessible, hence none of the two cases can be excluded based on this data.

Despite of the diamagnetic character of the Ni ion, we find a similar

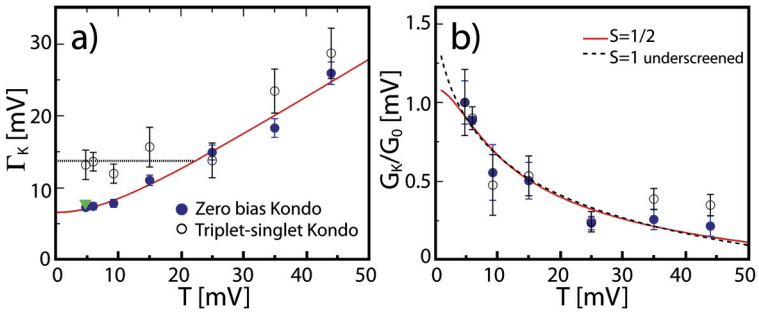

Figure 5.6.: Temperature dependence of a) the width (Γ_K) and b) the intensity (G_K) normalized to the intensity at 5 K (G_0) of the elastic Kondo resonance. A Kondo temperature of T_K = 27 $\pm$ 2 K is obtained by fitting Γ_K with Eq. Equation 3.21 (solid line). The (green) triangle in a) corresponds to the data obtained for NiPc at 5 K. The solid (dashed) line in b) is a fit of G_K/G_0 for the S=1/2 (underscreened S=1) cases of Equation 3.22.

peak at E_F for NiPc. This establishes that the origin of the molecular spin inducing the Kondo resonance is not based on the TM. A Kondo temperature of T_K = 29 K can be estimated for this molecule from the width obtained at 5 K (green triangle in Figure 5.6a). In addition, the intensity of the resonance in both CuPc/NiPc is not centered at the TM ion, but rather follows the spatial distribution of the $2e_g$ and $2e_g$+U, as revealed by the similarity of their dI/dV maps (Figure 5.3 and Figure 5.5e,f). These two observations make it clear that the interacting spin is indeed localized at the ligand. A result in perfect agreement with our STS observation of a single electron charge transfer to the $2e_g$. Furthermore the experimental values we obtain for the energy of the singly occupied level (ϵ= -0.3 eV), its width ($\Gamma \sim 0.30$ eV), and Coulomb repulsion potential ($U = 0.65$ eV) confirm that we are indeed in the Kondo regime $|\epsilon|, |\epsilon + U| \geq \Gamma$ (see chapter 3) .

The direct observation of the "Coulomb blockade" peaks and the Kondo resonance allows, unlike previous studies of molecular adsorbates, for a univocal identification of the MO associated to the unpaired spin. As the spin participating to the many-body Kondo state originates from a single orbital, we expect a well-defined value of T_K over the whole molecule, which is confirmed by our observations. This is in contrast with the variations of T_K found for Co porphyrins adsorbed on Cu(111) that suggest

a spatially-dependent, multiple orbital origin of the Kondo interaction, possibly due to strong intermixing of TM and ligand orbitals near E_F [176].

5.3.1.1. Coupling of the Kondo resonance to vibrational and spin excitations

Apart from the Kondo resonance peak the spectra for NiPc and CuPc show multiple inelastic features. It is well known that inelastic excitations induce step-like increases in the differential conductance spectra symmetrically distributed in energy [188, 189], very much like the ones observed in the TM spectra of Figure 5.7. In Kondo systems, the coupling of the Kondo state to such excitations leads to additional peaks (K_v and K_{ts}) that appear locked at the same energies [190]. The origin of such side peaks in small aromatic molecules is restrained to vibrational or magnetic excitations, as was discussed in subsection 3.4.3 on page on page 49. The cotunneling mechanisms behind each process are presented in Figure 5.8.

We can assign the inelastic features found at the TM centers to vibrational excitations by comparing their energies with Raman vibrational modes of the gas-phase CuPc [191], as illustrated in Figure 5.7a.

Note that the vibrational spectra of NiPc and CuPc are nearly identical, as shown by the twin d^2I/dV^2 spectra displayed in the bottom graph. The step-like and peak-like contributions to the inelastic conductance can be obtained by fitting the dI/dV spectra with step and Lorentzian functions, as shown in Figure 5.7. From the fit of the spectra we observe that both NiPc and CuPc present more intense conductance steps at negative bias and more intense Kondo peaks at positive bias. These inverted correlation between vibrational and Kondo features has also been observed for TCNQ molecules adsorbed on Au(111), and has been attributed to the competition between the purely inelastic channel and the one including the Kondo effect [94].

At the benzene ring in contrast to the spectra at the TM ion, inelastic features appear only for CuPc (shown in Figure 5.7b). Since both molecules share the same vibrational spectrum the divergence must come from the magnetic configuration. Here the difference between the two is the additional magnetic moment in the Cu^{2+} ion, which coexist with the ligand spin in CuPc. We therefore assign these peaks observed in CuPc to intramolecular magnetic spin coupling, i.e., the coupling of the π-spin to

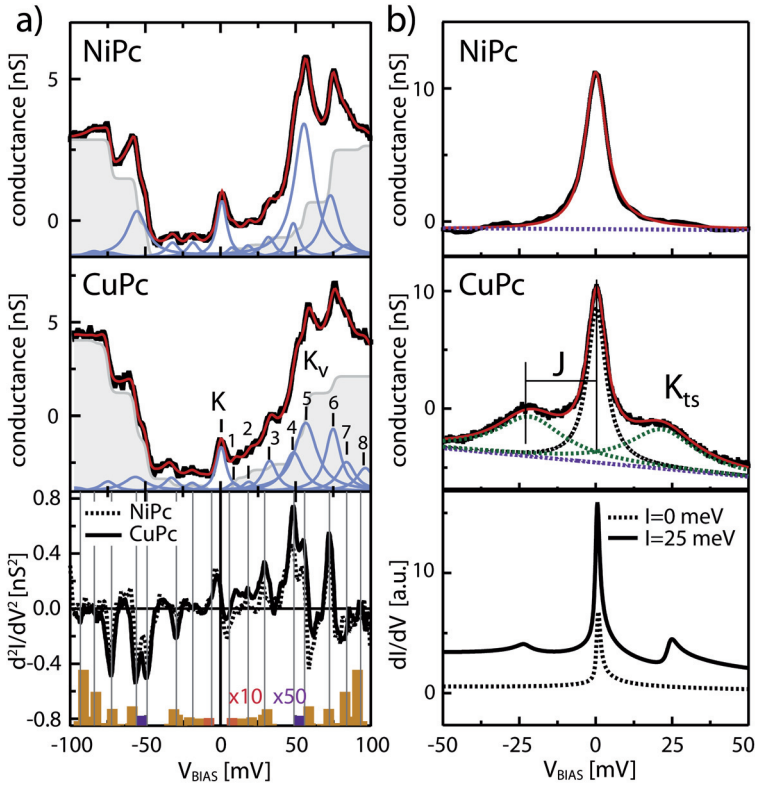

Figure 5.7.: Fit of the differential conductance (dI/dV) spectra of NiPc and CuPc measured at a) the TM ion and b) the benzene ring, using Fano functions and Lorentzian for the zero and finite bias peaks respectively, and step functions for the inelastic conductance steps observed at the TM ion. The bottom graph in a) is the second derivative (d^2I/dV^2) measured at the TM ion. The energies obtained from the fit are indicated by dashed lines in the d^2I/dV^2 spectra. The bars correspond to the intensity of calculated Raman (yellow) and infrared (grey) modes of gas-phase CuPc [191]. The bottom graph in b) show the theoretical PDOS obtained for the $2e_g$ with our ab-initio model, for I = 25 meV (solid) and 0 meV (dashed). The $2e_g$ on-site energy is ϵ = -0.35 eV, and the spectral density of the coupling with the substrate is assumed to have rectangular shape with magnitude Γ = 0.1 eV and band half-width of 10 eV (see Ref. [192] for more details).

the d-spin forming a singlet (S=0) and a triplet (S=1) state. The transition between the two states is equal to the energy of the side peaks indicating an intramolecular exchange coupling of $J = 21 \pm 1$ meV. The fact that an intense Kondo peak is observed at zero bias indicates a magnetic (S=1) ground state in the molecule, otherwise no Kondo screening would be possible. We thus conclude that the metal and ligand spin are aligned parallel to each other, which is supported by the gas-phase calculation of the magnetic moment of charged molecules presented in subsection 5.3.2 on page 99.

Underscreened Kondo effect in CuPc

Although the magnetic configurations of CuPc (S=1) and NiPc (S=$\frac{1}{2}$) are different, the two molecules exhibit similar Kondo temperatures. This can be understood by considering that in CuPc only the ligand spin couples to conduction electrons of the substrate, providing a single screening channel. The effective decoupling of the b_{1g} ($d_{x^2-y^2}$) orbital, confined in the molecular plane, leads to an underscreened Kondo state, meaning that only part of the total spin S=1 is screened and is reduced to S=$\frac{1}{2}$ [25, 100, 193]. This is part of a two-stage process, where the presence of a strongly-coupled and a weakly-coupled screening channel implies the existence of two different Kondo energy scales [100, 193]. In the temperature range accessible to our experiment, only the $2e_g$ screening channel is effective, which explains why the measured Kondo temperature is similar for CuPc and NiPc. The fit of the intensity of the Kondo resonance using the analytic expressions $G_K(T)$ derived from renormalization group theory for the S=1/2 and for the underscreened S=1 Kondo effect [25] does not contradict this interpretation (Figure 5.6b). Our measurements indicate that the residual spin of CuPc spin is not screened until temperatures much lower than 5 K.
Hence, the Kondo interaction in both molecules occurs only via the $2e_g$ spin, but in CuPc the latter is also coupled to the ion spin, as revealed by the spin excitations observed in the Kondo effect. These excitations have been correctly reproduced by R. Korytar and N. Lorente by using a multiorbital NCA model [192], as can be seen in Figure 5.7b.

Spatial distribution of inelastic excitations

The coexistence of vibrational and triplet-singlet Kondo excitations together with the spatial resolution of STS allow us to map the spatial dis-

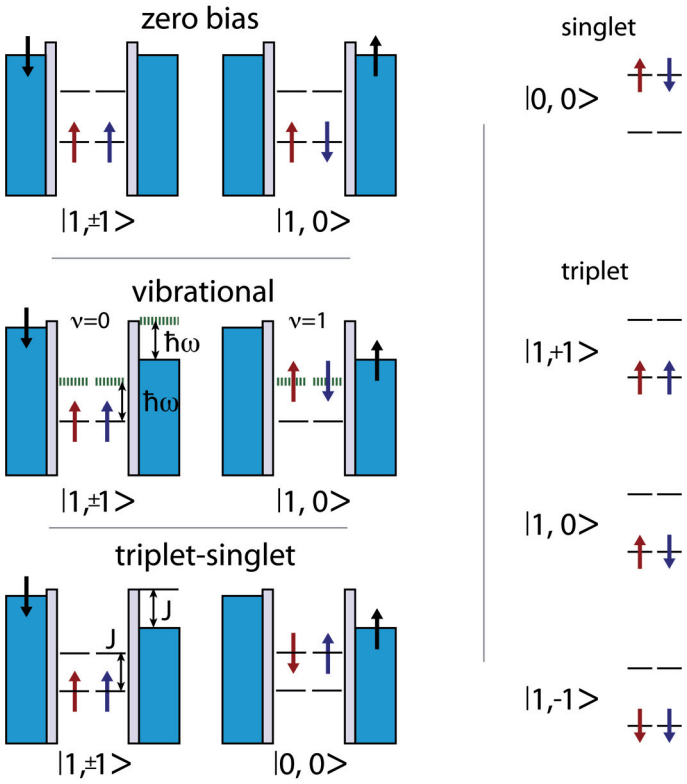

Figure 5.8.: Three types of inelastic excitations: i) The first event is the zero bias Kondo spin flip scattering occurring between the ligand spin and the Fermi sea electrons of the substrate (see chapter 3). This event occurs in NiPc and CuPc molecules, and creates the characteristic Kondo resonance at 0 bias, i.e., E_F. ii) The second event is found in both molecules: a coupling to vibrational nodes of the molecule. iii) the coupling between the two spins in the CuPc means a transition from the triplet ground state $|1\rangle$ to an antiparallel spin singlet orientation $|0\rangle$. The red arrows indicate the ion spin (only for CuPc), the blue ones the ligand (for NiPc/CuPc). $|S, m_s\rangle$ represents the spin state of the system.

tribution of each type of inelastic Kondo excitation for CuPc. In Figure 5.9 a series of spectra taken along a CuPc molecule, starting from a benzene ring up to the TM center are shown. The data shows that the vibrational and triplet–singlet inelastic channels occupy mutually exclusive regions

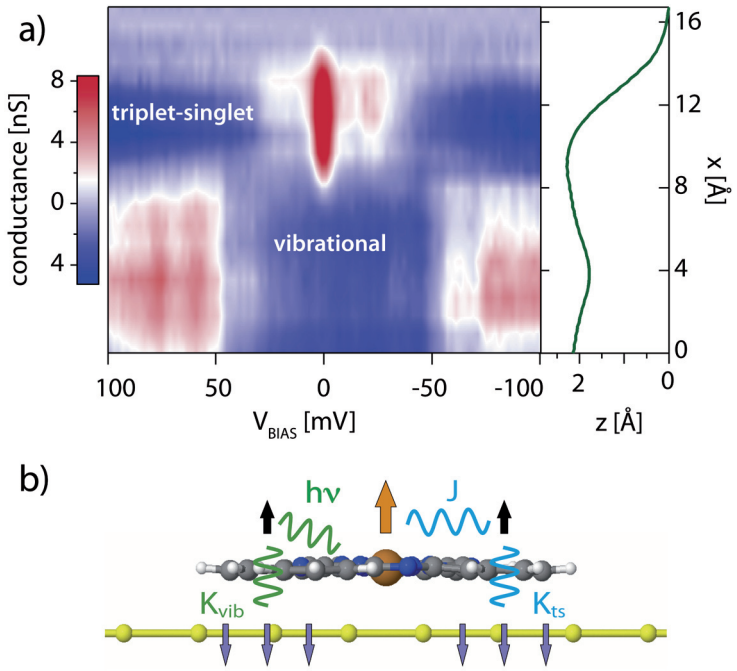

Figure 5.9.: a) dI/dV spectra acquired along a CuPc molecule revealing the different localization of the vibrational and triplet-singlet Kondo resonances. The position of each spectra is indicated by a topographic linescan below. b) Schematic representation of the different coupling mechanisms behind each inelastic Kondo process.

both in energy and space, with the former localized on the central part of the molecule and the latter on the external ring structure.

The localization of the vibrational coupling around the ion site can be understood on the grounds that the distortion of Cu–N bonds in all excited modes are the vibrations that we observe [194].

On the other hand, the intensity of the triplet–singlet excitations is proportional to the local spin/charge density as well as to the probability to tunnel to spin-polarized orbitals, the latter being much higher for the $2e_g$. Thus, as the STM tip has the role of a mobile electrode, our measurements show that the appearance of nonlinear resonances in the I/V curves of metal–organic complexes is related in a nontrivial way

to the contact geometry with the metal leads and to the vibronic and magnetic degrees of freedom within the molecules. The same reasoning applies to the zero bias Kondo peak itself, whose intensity mimics that of the $2e_g$ (See Figure 5.5). Note that the two inelastic peaks exhibit a sharp spatial separation of around 1 Å. This spatial contrast reflects how the atomic configuration of a molecule-metal junction determines not only the resonant transport through MOs, but also the type of inelastic processes that dominate transport at the Fermi region.

Relaxation and universal scaling of nonequilibrium Kondo excitations.

The spin and current dynamics in small quantum objects coupled to external charge reservoirs are difficult to describe theoretically. This is especially true for systems where different many-body excitations are present [195]. Up until now this problem has been difficult to address experimentally. However we observe multiple relaxation channels for the CuPc ligand spin, related to nonequilibrium Kondo processes caused by vibrational excitations at energies E_{Kv1}, E_{Kv6} and a triplet–singlet transition at E_{Kts}. Hence CuPc provides the opportunity to compare spin relaxation via vibrational and magnetic cotunnelling events in the same molecule.

To do so, we deconvoluted the inelastic tunneling conductance of purely vibrational origin from the vibrational Kondo finite-bias intensity by fitting the dI/dV spectra of CuPc and NiPc using the sum of six-step functions and Lorentzian curves on each side of E_F (Figure 5.7 a). The triplet–singlet excitation features were modeled by two Lorentzian peaks as shown in Figure 5.7b.

The full width at half maximum of the triplet–singlet peaks (Γ_{ts}) and vibrational resonances (Γ_v) is inversely related to the decoherence time of the cotunnelling processes schematized in Figure 5.8. At temperature $T \geq T_K$, both Γ_{ts} and Γ_v are dominated by thermal broadening, similar to Γ_K. Deeper into the Kondo regime at $T < T_K$, however, we observe that Γ_{ts} deviates from Γ_K, saturating at 14 meV (Figure 5.6a). This implies that the intrinsic timescales of triplet–singlet and zero-bias Kondo spin flips are different. These findings led us to investigate the scaling properties of the conductance as a function of T_K and V_b. Current theoretical models state that nonequilibrium Kondo physics is completely universal and determined by a single energy scale corresponding to T_K

(ref. [196]). This universality, however, applies uniquely to the elastic Kondo resonance, hence there is no physical reason for Kondo processes that involve different type of inelastic excitations to obey the same decoherence rate as a function of energy.

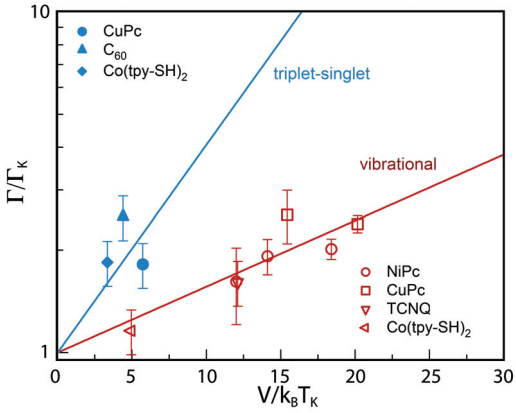

Figure 5.10.: Spin versus vibrational relaxation channels. Normalized width Γ/Γ_K of the inelastic Kondo resonances as a function of V_b/k_BT_K. Data for CuPc and NiPc are compared with that for other molecules for which either spin or vibrational Kondo excitations have been separately reported. Triplet–singlet (cyan) and vibrational (red) Kondo excitations separate into two groups. Exponential fits (solid lines) evidence the different contribution of each process to the decoherence rate. Data from C_{60} [101], Co(tpy-SH)$_2$ [25, 22] and TCNQ [94].

A major hurdle to prove this point lies in the need of comparing data relative to triplet–singlet [25, 101] and vibrational excitations [22, 94] for different systems, especially in experiments where the electrode–molecule coupling and Kondo temperature greatly differ from each other. Such a comparison can be carried out by renormalizing both Γ and V_b by the relevant Kondo energy scales for each system that is, by plotting Γ/Γ_K as a function of V_b/k_BT_K, in analogy with the theory of dc-biased quantum dots [196]. Figure 5.10 shows the renormalized Γ_{ts} and Γ_v values of CuPc and NiPc, obtained in this way. We find that Γ_v follows the exponential trend with V_b expected for the relaxation of nonequilibrium Kondo processes that are dominated by electron-hole pair excitations [100, 197]. However, Γ_{ts} of CuPc lies outside this trend, showing a larger normalized

decoherence rate compared to vibrational excitations.

By including data from literature experiments, with T_K differing by as much as two orders of magnitude, reporting singlet-triplet [25, 101], or vibrational [22, 94] Kondo features, we further support this conclusion.

Figure 5.10 shows that finite-bias resonances related to vibrational excitations fit a single exponential curve (red line) with a decay rate that is a factor 3 smaller compared with inelastic spin excitations (cyan line), reflecting the different decay channels present in each case. We conclude that the coherence of non-equilibrium Kondo cotunnelling events is universal only when restricted to the subspace of a given observable. Indeed, the faster decoherence, observed for the triplet-singlet channel, can be related to the higher coupling of the electron bath to spin excitations as compared with phonon excitations [189], and might apply to other types of nonequilibrium Kondo phenomena, including those involving Cooper pairs or photon adsorption [102, 103].

5.3.2. DFT: magnetic structure

By calculating the saturation magnetic moments of different MePc, DFT provides complementary results to the analysis of the Kondo spectra reported above. Moreover, in addition to supporting the interpretation of our STS data, DFT allows us to construct a quantitative picture of the effect of the different charge transfer mechanisms on the molecular magnetic properties.

	ΔN	m^{gas}_{MPc}	$m^{gas}_{[MPc]^-}$	m^{ads}_{MPc}
FePc	0.80	2.00	1.00	1.06
CoPc	0.99	1.00	0.00	0.63
NiPc	1.13	0.00	1.00	0.14
CuPc	0.81	1.00	2.00	1.32

Table 5.1.: Computed charge transfer ΔN (in electrons) and total magnetic moment m (units of μ_B) in neutral and anionic gas-phase, and adsorbed molecules, calculated by GGA+vdW.

Table 5.1 summarizes the magnetic moments calculated for the neutral

and anionic form of gas-phase MePc as well as for MePc adsorbed on Ag(100). Although the amount of charge transferred from the substrate to the molecules is similar in all cases, the total magnetic moment is reduced in FePc and CoPc, whereas it is increased in NiPc and CuPc with respect to the neutral gas-phase MePc. The calculations confirm that the magnetic moment of the TM ions in NiPc and CuPc is not perturbed upon adsorption, due to the small hybridization of the planar b_{1g} orbital with the substrate states. This is in agreement with previous results obtained by XMCD on CuPc/Ag(100) (see Figure 5.11) and with the coexistence of TM and ligand spins in CuPc deduced from the Kondo spectra. We recall that, the ligand spin is barely present in the calculations with adsorbates due to the underestimation of correlation effects in DFT. For NiPc, we calculate a small magnetic moment of 0.14 μ_B, while for CuPc the moment is just slightly larger than the 1 μ_B corresponding to the unpaired spin in the b_{1g} orbital.

Since the charge transfer is close to one electron, one way to estimate the magnitude of the ligand spin using DFT is to consider gas-phase anions as a model of an adsorbed MePc. Here the number of electrons belonging to the molecule is fixed and the calculations can be constrained to yield the minimum energy spin state. Figure 5.12 displays the spin density of neutral and anionic gas-phase molecules, where we clearly observe the additional ligand spin of NiPc and CuPc upon charge transfer. In CuPc, the spin density originating from the b_{1g} orbital is also observed, distributed over the Cu ion and N_p atoms.

FePc and CoPc present a more complicate picture compared to the simple addition of one spin in NiPc and CuPc, partly because of the strong hybridization with the substrate discussed in subsection 5.2.2. In both cases, the magnetic moment is reduced upon adsorption. The extra electron donated by the surface is not easily assigned to a single MO, inducing a reorganization of the charge within the molecule.

The results obtained for gas-phase anions can be used to disentangle the different mechanisms responsible for the quenching of the magnetic moment. As shown in Figure 5.13, the spin density of FePc follows the same distribution in the gas-phase anion and in the adsorbed molecule. This resemblance is also confirmed by comparing their element-resolved magnetic moments in Table 5.2, which are very similar in both cases. Thus, regardless of the strong hybridization of adsorbed FePc, the main features of the spin moment distribution are again captured by the simple addition

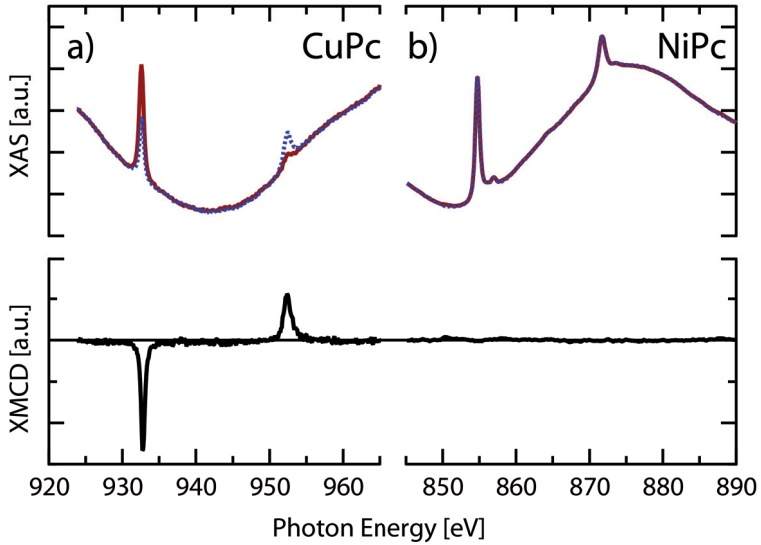

Figure 5.11.: XMCD measurements of molecular films in the submonolayer regime on Ag(100) a) CuPc film: showing an XMCD signal for Cu edge, indicating that the Cu ion retains its moment. b) NiPc film: no XMCD signal is observed, meaning that the Ni is non-magnetic in the NiPc/Ag(100) configuration. Measurements taken at T=8 K, normal incidence and 5 T applied field at the ID08 beamline of the ESRF. For more details see [198].

	m_M	m_N	m_C	m_{tot}
FePc_{gas}	1.94	-0.13	0.19	2.00
$[\mathrm{FePc}]^{1-}_{gas}$	2.04	-0.31	-0.73	1.00
$\mathrm{FePc}_{Ag(100)}$	2.14	-0.26	-0.82	1.06

Table 5.2.: Computed element-resolved magnetic moment m (units of μ_B) for FePc in the neutral and anionic gas-phase, and in the adsorbate, using GGA+U.

of one electron to the gas-phase system. The true nature of the ground state of FePc on Ag (100), however, is most likely more complex than suggested by the calculated spin density distribution, due to the interplay of several MO close to E_F and dynamic electron correlation effects that are not included in DFT. The computed electronic structure for FePc yields

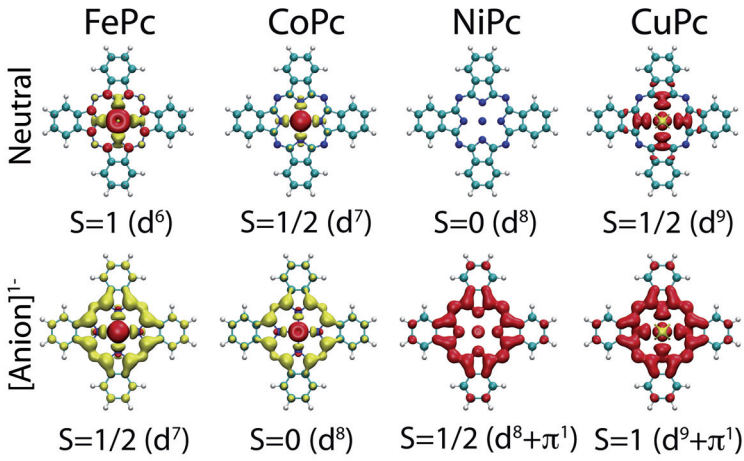

Figure 5.12.: Spin density of neutral (top) and anionic (bottom) gas-phase MePcs. Red/yellow indicate spin up/down.The isovalue for the spin density is 0.005

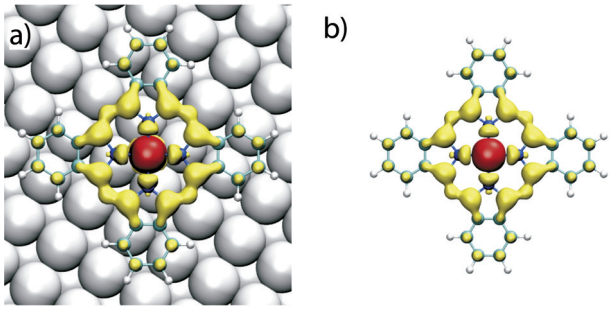

Figure 5.13.: Spin density distribution of FePc a) adsorbed on Ag(100) and b) in the gas-phase anion. Red/yellow indicate spin up/down. The iso value for the spin density is 0.005 in both cases.

a S=1/2 system when adsorbed on Ag (100), same as for the gas-phase anion. However, the adsorbate exhibits a more complex configuration due to the presence of multiple molecular orbitals at the Fermi level. This could result in either a mixed-valence system, given the Fermi level crossing and strong interaction of the a_{1g} orbital with the substrate, or a more complex Kondo behavior with a low-temperature Kondo phase originating

in the many less-coupled orbitals near the Fermi energy. This complex behavior makes FePc/Ag(100) an interesting candidate to study very low temperature Kondo physics in a multi-orbital system.

CoPc represents another case of nontrivial charge transfer occurring upon adsorption. For example, the a_{1g} orbital is filled, but new empty d_π states appear above E_F, as shown in Figure 5.2b,c). Moreover, the gas phase anion is not a good model for the adsorbed molecule. As shown in Table 5.1 and Figure 5.12, the anion is in a S=0 state, due to antiferromagnetic coupling between spins residing in different MOs, while in the adsorbed case we find a non-integer spin magnetic moment of $0.63\mu_B$. This non-integer spin, together with the absence of a Kondo interaction, could indicate that CoPc is in the mixed-valence regime, with charge fluctuating between the CoPc d and Ag states, similar to the results obtained for CoPc on Au(111) using x-ray absorption spectroscopy [170].

5.3.2.1. Intramolecular spin correlation

The TM ion-ligand spin coupling observed via the inelastic Kondo interaction in CuPc can be studied in gas-phase $[\text{CuPc}]^{1-}$. Here, the energy of ferromagnetic and antiferromagnetic spin configurations can be computed by fixing the total spin of the molecule. The ferromagnetic (triplet) alignment is favored over the antiferromagnetic (singlet) one. The triplet ground state agrees with the experimentally observed zero-bias Kondo resonance. From the energy difference between triplet and singlet states, evaluated using the parallel spin ($E_{\uparrow\uparrow}$) and antiparallel spin ($E_{\uparrow\downarrow}$) energies, and taking the correct singlet and triplet configurations to yield $J = 2(E_{\uparrow\downarrow} - E_{\uparrow\uparrow})$, the exchange coupling constant J for the anion can be extracted, we find $J = 38$ meV. The discrepancy with the experimental value $J = 21$ meV for CuPc/Ag(100) can be explained by surface screening, which is expected to significantly reduce exchange correlation effects involving hybridized orbitals.

The distribution of spin density in $[\text{FePc}]^{1-}$ and $[\text{CoPc}]^{1-}$ shown in Figure 5.12 reveals a different type of intramolecular spin correlation. Both neutral and anionic molecules exhibit antiferromagnetically aligned TM ion and ligand spins, indicating that the contrast is not related to new spins induced by the substrate, but is intrinsic to the molecule. It is derived from the original TM ion spin, which extends to nearby C and N atoms upon the formation of mixed MOs with mixed d- and π-character. This intramolecular antiferromagnetic spin coupling is a result of the large

exchange splitting of the d-levels of the Fe and Co ions. This induces spin-dependent mixing of the d and ligand states, leading to the formation of spin-polarized MOs with different spatial distribution. The site- and energy-dependent spin contrast recently measured for CoPc deposited on Fe(110), with a total molecular moment of zero, can be explained by a similar mechanism [174].

5.4. From clusters to monolayer

As we have seen, the electronic and magnetic characteristics of single MePc molecules are strongly influenced by their interaction with the surface. Intermolecular interactions can, however, play a role as well. Previous experiments found a decoupling caused by increased molecular coverage, for instance an STM study of a FePc monolayer on Ag(111) showed that intramolecular interaction, leads to sharper single resonances in STS [129]. Photoemission experiments for CuPc on Ag(111) also came to this conclusion [199].

Here we investigate this in more detail by increasing the number of neighboring molecules step-by-step, and their effect on the evolution of the electronic structure. CoPc and CuPc molecules serve as model systems for the main hybridization channels through ion's d states and the ligand orbitals respectively. We will see that the interaction with the surface through the more delocalized ligand states, as is the case for CuPc is strongly influenced by intermolecular forces, leading to a complex changes in the electronic structure. In contrast for CoPc, the interaction through hybridized d states is inert.

5.4.1. Small clusters of CuPc

To systematically investigate the influence of neighboring molecules on the electronic and magnetic structure, we studied small CuPc clusters. Using the lateral manipulation capabilities of our STM, we created several cluster geometries, with different nearest neighbor configurations, in a controlled and reproducible way (see Figure 2.8 on page 27). We ensured that the molecules remained unperturbed and in the same adsorption configuration after manipulation by comparing topographic images and conductance spectra before and after their displacement.

In a linear cluster consisting of four CuPc, (shown in Figure 5.14a) the two molecules at the end have 1 nearest neighbor (NN), while the two central ones have 2 NN. We investigate the impact of NN on the electronic structure by dI/dV maps and STS.

The STS for molecules with 1 NN is very similar to the single molecule spectra; the occupied and unoccupied MO around E_F are still present as well as the Kondo resonance. We observe a small upshift of the charged peak, previously attributed to the $2e_g$ state (see Figure 5.14b). The spatial distributions of the states found above and below E_F differ however. The two dI/dV maps taken at -150 mV and 400 mV are orthogonal to each other, indicating that they not caused by the same state anymore. The 2 fold-degeneracy, not considering the spin, of the $2e_g$ state hence is broken by the interaction with the neighboring molecule. The two new states have a different symmetry: singly occupied molecular orbital α_{2eg} and the unoccupied β_{2eg}.

The electron that is transferred from the substrate is located in the α_{2eg}, which together with its unoccupied counterpart the $\alpha_{2eg} + U$ is now responsible for the Kondo interaction. This can be seen by the change in the symmetry of the Kondo intensity distribution, which follows the α_{2eg} distribution, and not that of the $2e_g$. This change coincides with a lowering of the Kondo temperature (see Figure 5.16).

The electronic structure of the two central molecules with 2 NN, shows no changes for the unoccupied states, the new β_{2eg} symmetry is maintained, as is its position in energy. The occupied states, however transform further; a new feature appears at ~ -60 mV, while the α_{2eg} remains barely measurable in the STS. The Kondo resonance is still visible, and has the same symmetry as for molecules with 1 NN albeit weaker, T_K is shifted further down (Figure 5.16). We can thus conclude that the single electron in the α_{2eg} is still the cause of the Kondo interaction. The origin of the new interface state feature is not clear. Nevertheless the existence of a Kondo resonance following the α_{2eg} symmetry, indicates that the feature at -60 mV is not a further upshift of the α_{2eg}, but rather an evolution of the electronic structure caused by the presence of the 2 NN.

To investigate molecules with more NN, we switch to a different cluster geometry. Figure 5.15 shows a 3x3 square cluster created from a larger self-assembled structure through lateral manipulation (see page 27). The central molecules on the sides have 3 NN while the center one has 4 NN. The dI/dV maps show changes occurring to both the occupied and un-

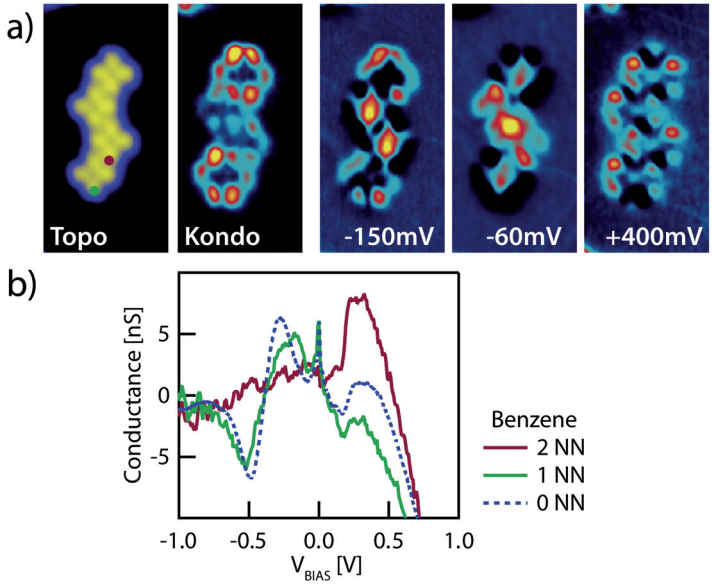

Figure 5.14.: a) STM topography of a 4x1 CuPc cluster, and dI/dV maps of STS resonances at the indicated energies. The Kondo map is measured using the d^2I/dV^2 signal at -6 mV. Note that the Kondo resonance can be observed for all four molecules, albeit weaker for the center ones. b) STS taken on the outer benzene of a CuPc with 1NN and on the bonding edge of a CuPc with 2 NN (-1 V, 3 nA).

occupied states. The very pronounced interface state at -80 mV has most intensity between the molecules in the cluster, whereas the α_{2eg} symmetry is not found below E_F. The β_{2eg} state is shifted upward form 300 mV to 650 mV for 3 NN and to 950 mV for 4 NN, its intensity distribution follows the symmetry of the bonding environment.
The Kondo resonance has disappeared (See Figure 5.16). Note that this change is reservable. By removing one of the corner molecules of the cluster two molecules change form 3 NN to 2 NN, and show the Kondo resonance again (Figure 5.15 right panel). The fact that the Kondo interaction can be "turned on" proofs that the molecules are all unperturbed.

Previous studies have shown that the Kondo temperature of metal-organic complexes can be manipulated by locally modifying the ligand field acting on the transition-metal ions [25, 112] or by screening the surface electron density around molecular adsorbates by other molecu-

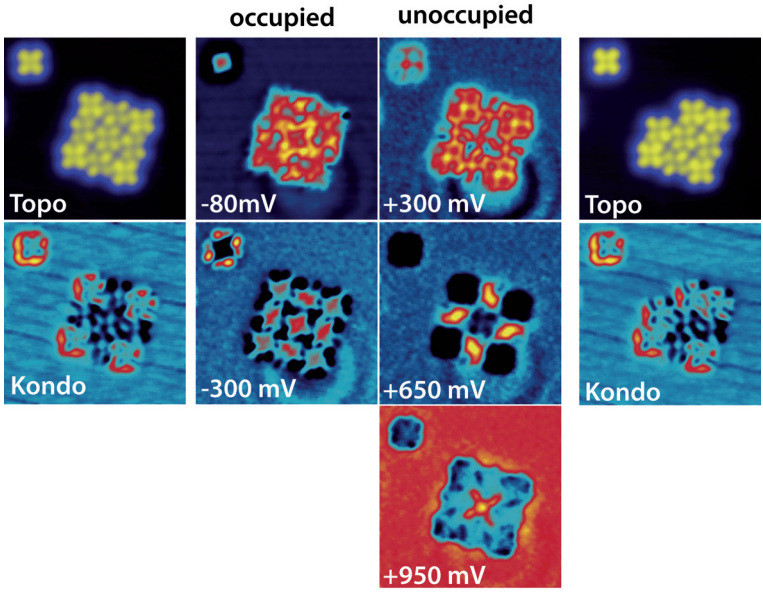

Figure 5.15.: STM images of a 3x3 cluster of CuPc before (left) and after (right) removing a corner molecule by manipulation with the tip: Topography and Kondo intensity distribution. Note that the Kondo resonance can be observed only for molecules with a number of lateral bonds smaller than three. The center panels show molecular orbital conductance maps.

les [200]. In our system, we observe a gradual lowering of the Kondo temperature with increasing NN, until the Kondo resonance completely disappears for molecules with 3 or more NN (Figure 5.16). It is difficult to specifically connect its disappearance with one of the two changes in the electronic structure: The emergence of a new state below E_F, or the decoupling of the molecule suggested by the upward shift of the β_{2eg}. In any case, both effects indicate a strong distortion of the original molecular states, as opposed to what we observe for single molecules.

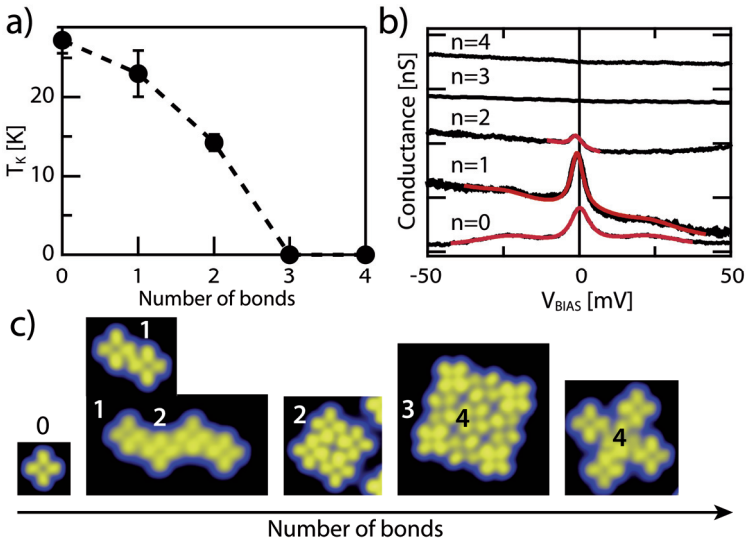

Figure 5.16.: a) Evolution of the Kondo temperature with the number of intermolecular bonds, obtained from Fano fits to the STS in b) STS conductance spectra acquired at 5 K at the benzene of molecules with different number of nearest neighbors and in different configurations. c) Examples of CuPc clusters used in the study of the dependence of the Kondo interaction on the number of intermolecular bonds. The number of lateral bonds to neighboring molecules is indicated.

5.4.2. Monolayers of CuPc and CoPc

CuPc monolayer

To complete the investigation of the influence of intermolecular forces on the electronic structure we investigate a close-packed monolayer of CuPc. Since the molecules in the monolayer are also in a 4 NN configuration, the STS curves are identical. The interface state at -80 mV has its maximum intensity between the molecules of the monolayer, as can be seen in Figure 5.17 in dI/dV maps and STS. The origin of this state however remains unclear for the monolayer.

For the unoccupied states, we observe a progression of sharp resonances, depending on where the STS was taken exactly: on the ion (650 mV), between the molecules (750 mV), and on the benzene (790 mV).

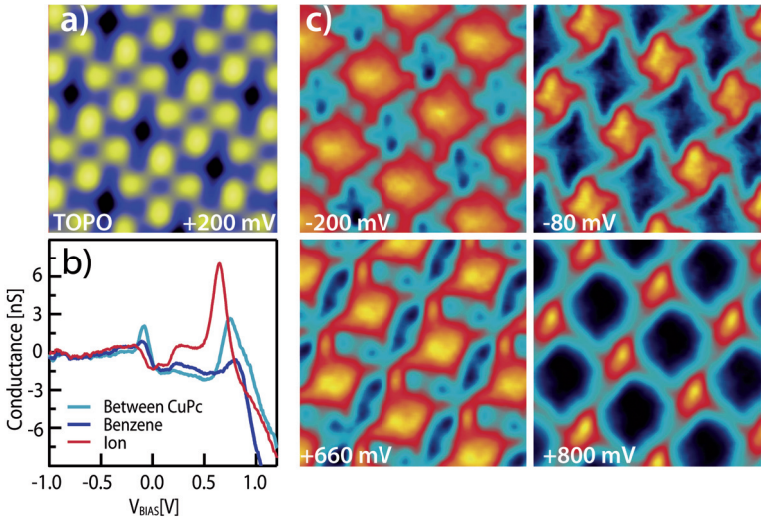

Figure 5.17.: Electronic structure of 1 ML CuPc/Ag(100). a) Topographic image obtained at 470 pA, 200 mV. b) STS spectra at different points of the molecule. The tunneling gap was set at 3 nA, -1V. c) STS maps of the same region, showing the molecular resonances near the Fermi level.

These peak energies show an extreme dependence on the tip height during the measurement. Kröger et al. have shown that, even within the tunneling regime of an STM, the electric field of produced by the tip can affect the energy position of the surface state, analogue to the stark effect [201]. Molecular orbitals sufficiently decoupled from the metal substrate and with the right alignment in the electric field, should also be shifted by this tip induced Stark shift [202].

The plot of the resistance against the peak position (Figure 5.18a) shows the characteristics of a linear Stark effect. This becomes even clearer when plotting the shift versus the electric field, using the method from Ref. [201]. The peak position versus tip height reveals a linear dependence -0.16 V/Å. The molecule with 4 NN in the 3x3 cluster (Figure 5.15) also shows this behavior, however with a higher shift of -0.28 V/Å, this variance is most likely caused by the different field created by different tips.

The origin of the position dependence of the unoccupied feature is not entirely clear. A topographic effect, combined with the observed stark shift, can be excluded. The topography indicates that the tip would move

towards the sample between the molecules, which for the Stark effect would indicate an upshift in energy, we observe however the reverse effect: the feature between the molecules lies lower than that on the benzene. A possible explanation might be related to a band dispersion due to hybridization with the upshifted surface state, as observed for PTCDA islands on Ag(111) [203, 204].

We would like to mention that in the dI/dV maps of the CuPc monolayer the chirality caused by the interaction with the substrate is still visible, and the decoupling does not affect it.

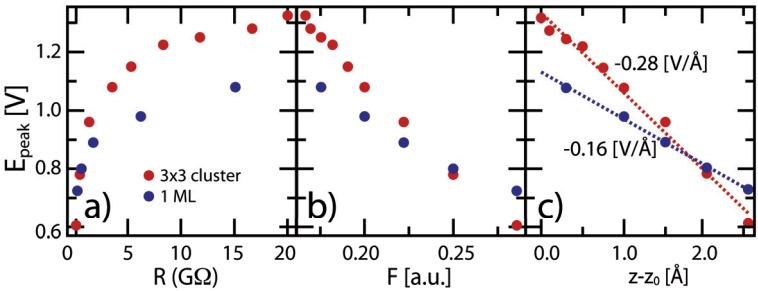

Figure 5.18.: Stark-shift of the LUMO level: a) Peak position vs. tunneling resistivity. b) Peak position vs. electric field, calculated after ref. [201] c) Linear relationship between z and the peak position. Positive z values correspond to a smaller tip-molecule distance. The tunneling gap was set at 15 pA, 0.4 V.

CoPc monolayer

In contrast to the pronounced changes occurring in CuPc cluster, the spectra for CoPc show no difference between the single CoPc and the monolayer (see Figure 5.19). CoPc does not decouple from Ag(100) by intermolecular interactions.

The coupling to the substrate in CoPc occurs mainly through the TM's d states, while for CuPc the ligand states are the main interaction channel (see Table 4.1 on page 60). The difference in behavior for CuPc and CoPc could be related to (i) the strength of the coupling which appears to be stronger for direct TM-substrate interaction, and (ii) the fact that intermolecular forces directly interact with the ligand orbitals, and hence could possibly weaken their coupling to the substrate.

The coupling strength, however, also depends on the substrate. Ref. [129] reports a decoupling for FePc monolayer on Ag(111) driven by intermolecular forces. FePc interacts with the substrate in roughly the same way as CoPc, through strongly hybridized d and ligand states. The interaction of absorbates with Ag(111) is weaker than with Ag(100), allowing the interaction between molecules to decrease molecule substrate coupling even for molecule of the FePc/CoPc type [129].

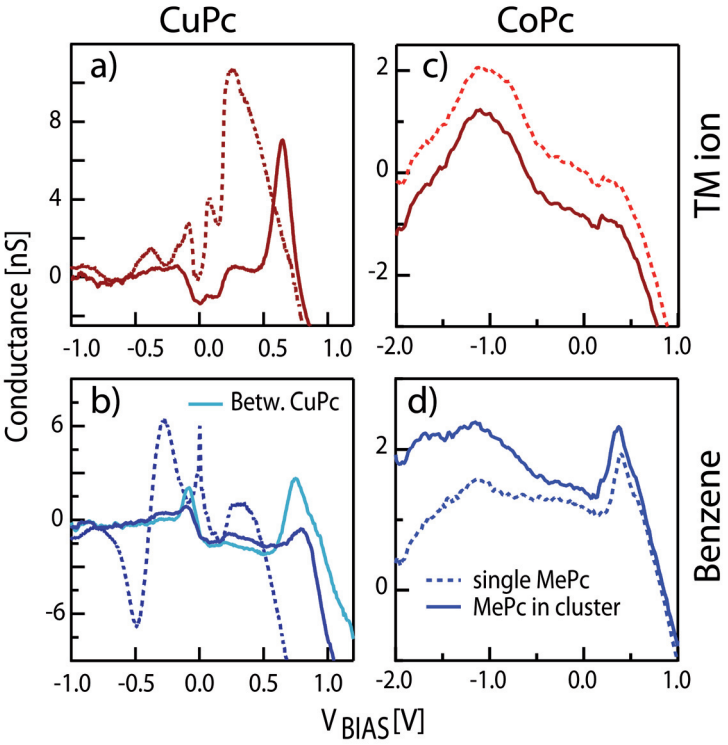

Figure 5.19.: STS spectra taken on CuPc and CoPc. Molecules inside a cluster (solid line), or single molecules (dotted line). STS was taken on the a) ion (red) of CuPc b) on the benzene ring of CuPc (blue), and between neighboring molecules (light blue). c) CoPc spectra taken on the ion (red) and d) on the benzene (blue). The gap was set to 3 nA,-1V for CuPc and to 2 nA, -2 V for CoPc.

5.5. CuPc multilayer

We have seen so far that MePcs absorbed on a surface are heavily influenced by the interaction with substrate. Molecular states are broadened and shifted by charge transfer and hybridization with the substrate. The electronic structure of a CuPc monolayer, where lateral molecular interactions become important, was still dominated by substrate-molecule interaction. In this section we will study the evolution of the electronic structure of CuPc stacked up to 5 molecular layers as it changes towards the semiconducting behavior of bulk CuPc. The influence of the substrate is gradually weakened by the lower lying molecular layers, and the molecules become more and more decoupled from the surface. We observe effects related to this decoupling such as sharpening of the molecular resonances [205, 206] and an increase in electronic lifetime leading to a coupling to molecular phonons [207]. For thick layers, a second tunneling barrier is created in addition to the vacuum region between the STM tip and the topmost molecule, leading to interesting phenomena caused by this double tunnel junction geometry, such as bipolar tunneling [208] and negative differential resistance (NDR) [209].

5.5.1. Molecules on higher layers - Spectroscopy

We performed STS measurements on CuPc molecules in different layers, the evolution of the spectra can be seen in Figure 5.20.

The STS taken on the second layer changes drastically compared to the monolayer spectrum. A gap opens around E_F, as peaks shift further apart. The onset of these features lie at -0.88 V and 0.86 V respectively, implying a gap of around 1.7 V. The conductance around E_F, however, is still not completely zero, and two weak and broad peaks are found at -0.28 V and 0.43 V. Furthermore, we observe that the peaks are generally shaper than those of the first monolayer. Especially the positive bias peak at 1 V is made up of three overlapping peaks. This multi-peak structure is caused by vibronic excitations, which have been observed for various molecules on insulating substrates [207, 208, 210], and will be discussed in more detail in section 5.5.1. The appearance of these effects, the gap opening and the sharpening of spectral features are clear signs that the molecules decouple from the surface [129]. However, the fact that two peaks lie in the gap indicates that this decoupling is not yet complete as these two peaks could be remnants of the interaction with

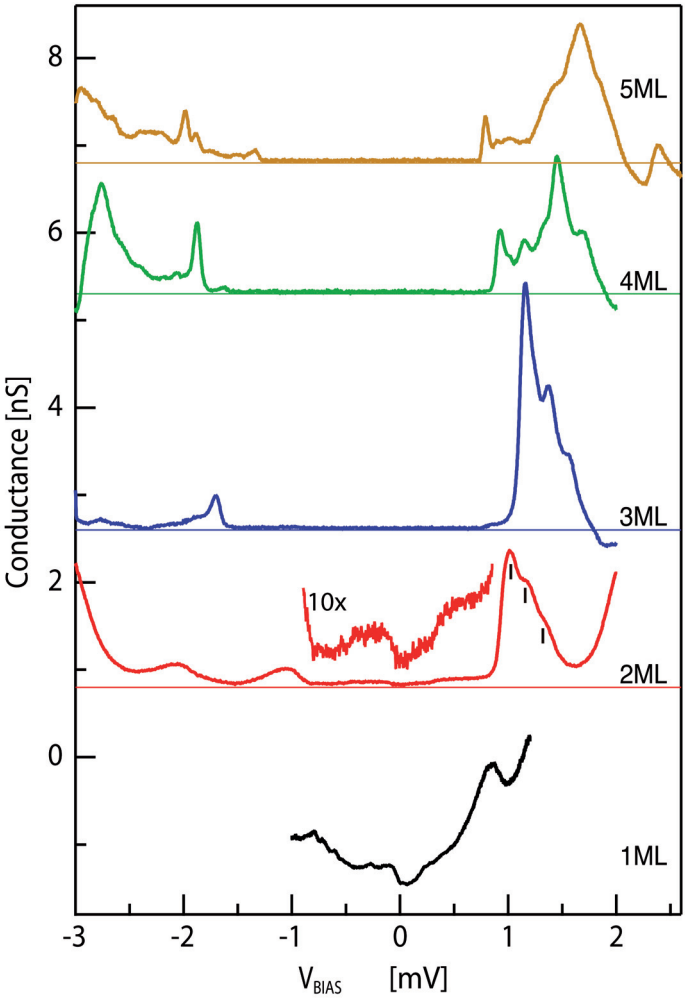

Figure 5.20.: Evolution of the electronic structure with film thickness. The gap increases, and vibronic features and NDR appear with increasing thickness, all signatures of an effective decoupling from the metallic substrate. All spectra are taken on the benzene part of CuPc, the vacuum gap was set to 0.2 nA, -3 V except for the 1 ML STS, for which 3 nA, -1 V was used.

the substrate or an interface state.

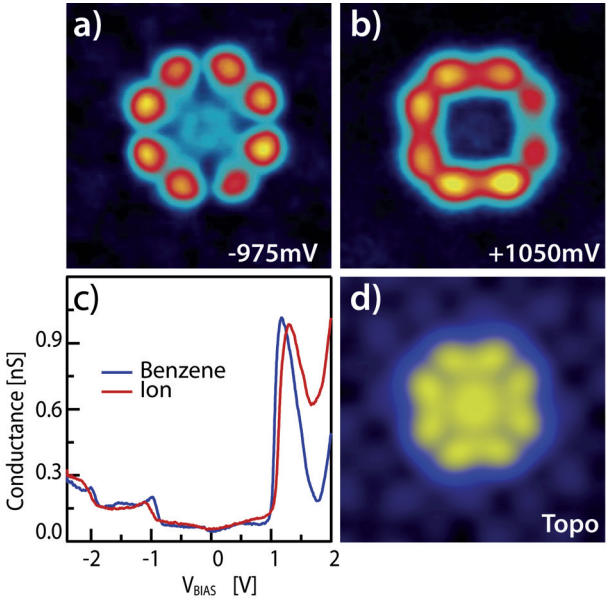

Figure 5.21.: a)-b) dI/dV maps of a single CuPc molecule in the 2nd layer. The HOMO and LUMO distributions are clearly visible for -975 mV and 1050 mV (5.3 nm x5.3 nm).c) STS taken on a single CuPc on the 2nd layer (0.2 nA, -3 V) d) A topographic image obtained during the acquisition of the dI/dV maps.

The weaker coupling to the substrate is such that is leaves main characteristics of the CuPc unperturbed, in contrast to what we have seen for single molecules and the monolayer. The magnitude of the gap (1.7 V) is very close to the HOMO – LUMO gap measured for thin CuPc films by PES/IPES (1.5 V [211] and 1.7 V [212]). Moreover, the spatial intensity distributions of the peaks at -0.97 V and 1 V, closely follows the LUMO and HOMO states for CuPc of Ag(100) (see Figure 5.3).

For molecules on the 3^{rd}, 4^{th}, and 5^{th} layer the spectra show additional changes. The sharpness of the peaks increases further, and the multiple peak at positive bias shows even more features. The gap between states significantly increases to roughly 2.5 V, while the STS signal inside the gap is zero. And lastly at the far positive end of the spectra we measure

negative differential conductance. The zero conductance gap, sharply defined vibronic features and the negative differential resistance (NDR) is are all feature that have been observed for molecules adsorbed on insulating layers [125, 207, 208]. Hence the two underlying organic layers decouple the molecules on the 3rd layer and above from the substrate.

Effectively there are now two tunneling barriers, the vacuum between tip and molecules, and the organic layers underneath. This situation makes it difficult to assign spectral features to MO and the wider gap has to be considered on these grounds. A certain part η of the bias voltage is dropped over the insulating layer, while the rest applies to the vacuum gap. The voltage drop can be modeled as a simple a plate condenser [125], if the thickness of the layer d, its dielectric constant ϵ, and the tip–sample distance z are known:

$$\eta = \frac{d}{(\epsilon z + d)} \tag{5.1}$$

This voltage drop makes both tunneling barriers voltage dependent. After ref. [125] the barriers will be given by:

$$B_{vacuum} = E_{vac} - E_{mol} + (1 - \eta)eV/2 \tag{5.2}$$

$$B_{layer} = E_{cond} - E_{mol} - \eta eV/2 \tag{5.3}$$

This means that one barrier will increase while the other will decrease with increasing bias voltage.

These voltage dependent barriers lead to bipolar tunneling, meaning that it is possible to tunnel through the same MO orbital at different bias voltages with opposite signs. Either the LUMO or the HOMO will be observed above and below E_F[*]. This depends on the ratio between the two barriers [207], and the distance of the HOMO/LUMO level to E_F [206]. For CuPc on thin NiAl oxide films, even the molecular adsorption conformation was found to influence, whether the HOMO or LUMO state

[*] In special conditions it is also possible to the see the LUMO above and the HOMO below E_F, similar to single tunnel barrier system [206].

was accessed in STS [208]. Unfortunately no values for the tip height z were measured during the experiment, so that the barriers cannot be quantified. This makes it difficult to determine if the observed states are related to the LUMO or the HOMO.

Moreover, the energy positions at which molecular resonances are observed, depend on the bipolar tunneling. Hence the observed widening of the gap is probably related to this phenomena, possibly in combination with screening effects due to the polarizable neighborhood of the molecules [129, 213, 214].

The NDR, observed in Figure 5.20 above 2 V is another effect caused by voltage dependent tunneling barriers in combination with sharp resonances and the absence of broad metallic states [215, 209]. Its presence further confirms the that molecule in the 3^{rd} layer are decoupled from substrate.

The fact that the spectra for the 3^{rd}, 4^{th}, and 5^{th} are relatively similar, except for intensity changes in the multi-featured peak, indicates that the decoupling form the substrate is completed on the 3^{rd} layer. As the tunneling rate, i.e., the current was kept constant between the spectra, effects due to the changing barriers thicknesses (higher molecular layers), were counteracted by adjusting the tip height z accordingly.

Vibronic progressions

The positive bias peak around 2 V is a multi-featured structure for the spectra taken on thicker layers. It was shown by W. Ho and co-workers [207, 208, 210] that a molecular orbital on an insulating layer can couple to vibrational excitation states, which will then be visible as equidistant peaks overlaying the actual molecular orbital. In these works the insulating layer was a thin NiAl oxide film. In our system already one molecular layer leads to a sufficient decoupling for vibronic excitations to be measured. With increasing layer thickness the quality of the decoupling increases and sharper and more vibronic peaks appear.

In multilayer CuPc all of the positive bias peaks for all layer thickness, can be fitted in this manner. Figure 5.22 shows the results of multi peak fits for the positive bias peak, revealing roughly equidistant peaks. We hence attribute the origin of these peaks in vibronic coupling to a MO. For each layer a slightly different energy spacing is found: 153 mV for the 2 ML, 155 mV for the 3 ML, 130 mV for the

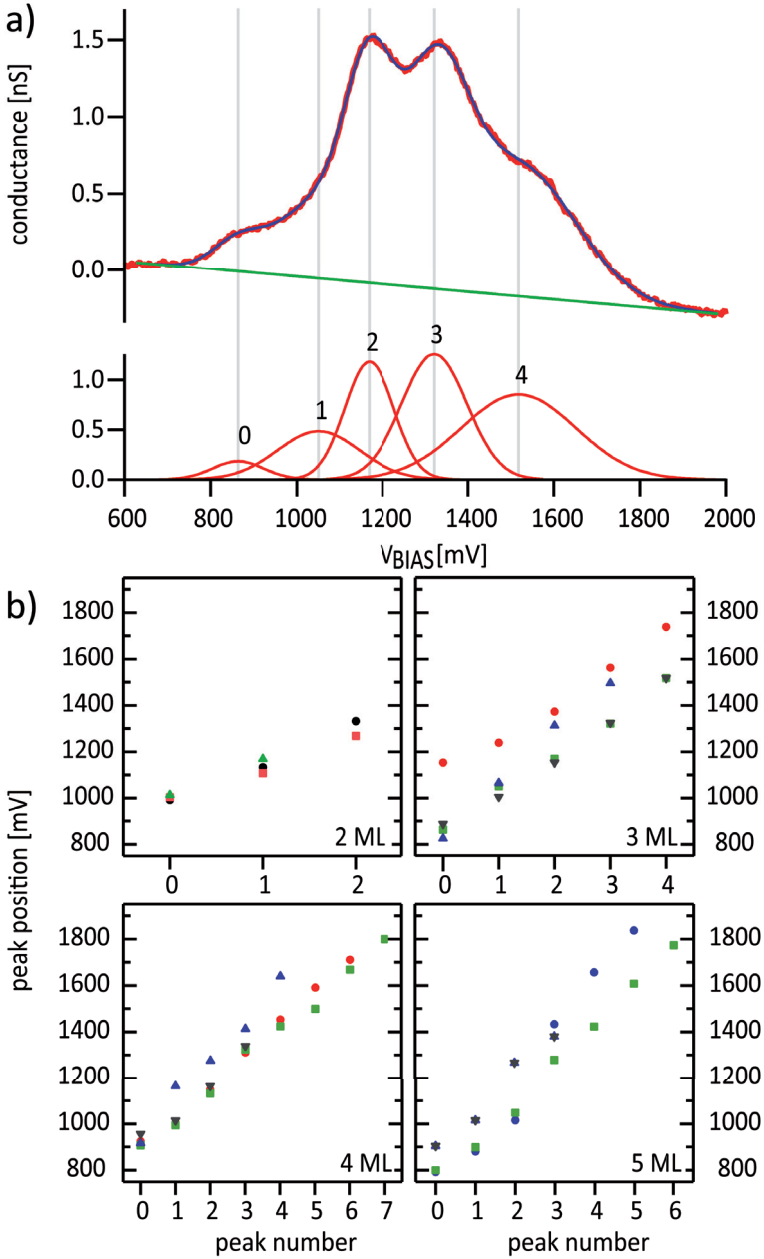

Figure 5.22.: a) Fit of the multi peak structure above E_F for 3 ML, the fitted peaks are presented. b) Peak position obtained from similar fits for the different coverages at different positions on the molecule, a roughly equidistant distribution is visible, pointing towards a vibronic origin of the multipeak structure. For the 3ML the red dots indicate the flat configuration, all other symbols mean tilted molecules.

4 ML and 172 mV for the 5 ML. Literature values for C-C or C-N stretching modes lie exactly within this energy range (150-200 meV) [216]. Furthermore PES measurements for thin films of CuPc on HOGP [216, 217], and in the gas-phase [218] show a vibronic coupling of the CuPc's HOMO to a vibronic excitation with 150 meV. The energy difference between the layers, is most likely due to the fact that these energy vales are also affected by the double tunnel junction and might vary by 5-20% depending on the exact geometry of the tunnel barrier [210].

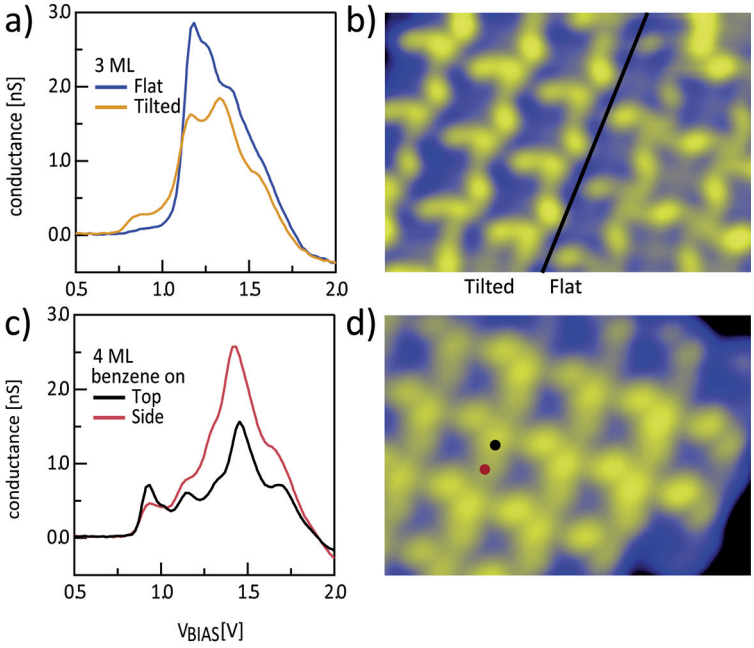

Figure 5.23.: a) STS taken on CuPc in the 3^{rd} layer in a tilted and a flat geometry (0.2nA,-3V), b) STM topography image showing the region with tilted and flat CuPc in the 3^{rd} layer (7 nm x5 nm, 10 pA, 1.5 V) c) STS spectra taken on the 4^{th} layer (0.2 nA, -3 V), the intensity of different vibrations shows a strong dependence on the site of the spectra d) STM Topography of CuPc in the 4^{th} layer indicating these points (7 nm x5 nm, 10 pA, 1.4 V).

We note that on the third layer part of the molecules lie flat, while others are already in the tilted geometry observed for the next layers. Spectroscopy taken on these two types of molecules on the 3^{rd} layer allows

us to study the effect of the tilt on the electronic structure (see Figure 5.23). Both spectra are very similar, however the onset of the positive bias peak has an enhanced feature in the tilted configuration. The fit of the complete multi-peak reveals that this peak forms part of the vibronic progression. In the panel for the 3 ML in Figure 5.22 it can be seen that the peak positions for flat (red dots) and tilted (all other) molecules are offset with respect to each other. The energy spacing for both geometries was found to be roughly 150 mV.

The 4^{th} layer shows another example of different intensities of the vibrational peaks. Here some of the benzene rings are in different positions, due to the tilted adsorption, leading to changes in the relative intensity of the vibronic peak changes depending on which benzene ring the STS was taken (see Figure 5.23c,d).

These two effects are related to the difference in molecular configuration, it is however not clear, whether it caused by changes in the Frank-Condon factors that determine the intensities of vibronic transitions, or by the tunneling barrier as with it the peak position, which was also found to be affected by the molecular configuration [208].

5.6. Summary

We studied the electronic and magnetic structure of four MePcs (Me = Fe, Co, Ni, Cu) adsorbed on Ag(100), investigating systematically the influence of the central metal ion on charge transfer, hybridization and magnetic properties.

Charge transfer and hybridization: The electronic structure of adsorbed MePc is modified mainly due to charge transfer from the substrate. Although all molecules receive approximately one electron, charge is transferred to the ligand $2e_g$ orbital in NiPc and CuPc, and to multiple MOs in FePc and CoPc, inducing internal charge reorganization. This difference is related to both energy level alignment and Coulomb repulsion. In addition the degree of hybridization of the MePc's d states is based on their spatial distribution, i.e., in-plane or out-of-plane. FePc and CoPc exhibit strongly hybridized $d_\perp$ states near E_F, whereas in NiPc and CuPc these states are shifted down in energy. The electronic configuration of the Ni and Cu ions is not significantly affected by adsorption, the $d_\parallel$ states remain unperturbed.

Reduction of the magnetic moment in FePc and CoPc: Both charge

transfer and hybridization tend to reduce the magnetic moment of FePc and CoPc. The computed electronic structure of FePc indicates a S=1/2 system when adsorbed on Ag(100), due to a spin density induced on the C and N atoms antiparallel to the Fe spin. The strong presence of MOs near the Fermi energy could indicate either a mixed-valence system, given the strong interaction of the a_{1g} orbital with the substrate, or a more complex Kondo behavior with a low-temperature Kondo phase originating in the many less-coupled orbitals near the Fermi energy. The non-integer moment obtained for CoPc and the existence of a substantial molecular DOS at the Fermi energy, together with the absence of a Kondo resonance in this molecule, suggest a mixed-valence configuration.

Additional magnetic moment in NiPc and CuPc: Opposite to the moment reduction in FePc and CoPc, the spin multiplicity is actually enhanced by charge transfer in NiPc and CuPc, due to the introduction of a ligand spin in the $2e_g$ orbital. This transforms NiPc into a paramagnetic molecule and induces a triplet ground state in CuPc, where the ligand spin is exchange-coupled to the ion magnetic moment.

Ligand Kondo effect in NiPc and CuPc: The interaction between the $2e_g$ ligand spin of NiPc and CuPc and the substrate gives rise to a Kondo interaction, which induces a prominent zero bias resonance delocalized over the perimeter of the molecules. In CuPc, the total magnetic moment is underscreened as the Kondo energy scale of the TM spin is orders of magnitude smaller than the one of the $2e_g$ ligand spin. However, the additional magnetic degree of freedom due to the TM spin leads to the coupling of Kondo and inelastic triplet-singlet excitations. The coherent coupling between Kondo spin flip and vibrational excitations induces inelastic Kondo resonances in both NiPc and CuPc.

Decoherence rate: The coexistence of different non-equilibrium Kondo processes related to vibrational and spin transitions in CuPc opens up the possibility to study the timescale and spatial localization of multiple spin excitation and relaxation channels within a single molecule. We find that the competition between Kondo, vibrational and magnetic excitations determines the decoherence rate of the molecular spin.

In general, we show that charge transfer and hybridization of MOs orbitals have profound effects on the electronic configuration, magnetic moment, and transport properties of metal-organic complexes adsorbed on a metallic substrate. Such effects in MePc do not only depend on the electronic configuration of the TM ions. Rather, the energy

position, symmetry, and spin polarization of the pristine MOs has to be considered within a comprehensive picture of the charge transfer process. Importantly, the magnetic moment of adsorbed MePc can be either reduced or enhanced depending on the relative energy of the $d_\perp$ and π-levels, and their degree of hybridization with the substrate. Further, the possibility of inducing additional ligand spins upon adsorption may be relevant to establish magnetic coupling in extended molecular structures assembled on metal surfaces.

Creating artificial clusters, we have studied in a bond by bond manner the influence of neighboring molecules of the electronic structure. For CuPc on Ag(100) we observe an evolution of the electronic structure, not a simple decoupling, highlighting effects due to lateral neighbors.
Evolution of the electronic structure: For CuPc already the interaction with 1 NN molecule leads to a break of the $2e_g$ degeneracy, into two orthogonal states, the partially occupied α_{2eg} and the unoccupied β_{2eg}. The ligand Kondo resonance, which is still caused by the single electron in the α_{2eg} and follows its intensity distribution. Starting with 2 NN a new state at ~ -80 mV, which is mainly located between the molecules is formed. The origin of this state remains unclear. CuPc molecules with 3 or 4 NN become more decoupled from the substrate, seen through an upshift of the β_{2eg}, and a Stark shift of the same orbital caused by the electric field of the tip. The β_{2eg} state shows a position dependence of its energy position, which might indicate a band formation caused by hybridization with an upshifted surface state.
Lowering of the Kondo temperature: The Kondo temperature is gradually lowered for each additional NN, until the Kondo resonance completely disappears for CuPc with 3 or more NN. It is difficult to assign the change in Kondo coupling to the decoupling or the formation of the new state.
No decoupling for CoPc: We do not see any difference between single molecule and a monolayer, due to the fact that the interacting states are localized at the metal ion and thus more protected from intermolecular interactions, and probably also due to the stronger molecule-substrate interaction than in CuPc.

To conclude we explored the electronic structure of of up to five molecular layers CuPc on Ag(100). We observe layer dependent decoupling from the substrate:

Partial decoupling for 2ML: Molecules on the second layer exhibit signs of a decoupling from the underlying substrate. A band gap opens between the HOMO and the LUMO, showing the literature magnitude of (1.7 V). The decoupling is however not yet complete, indicated by weak features within the gap.

Complete decoupling from 3ML: From the 3^{rd} layer on, the molecules become decoupled form the substrate, as evidenced by sharp spectral features, the appearance of a double barrier junction with voltage depended tunneling barriers, leading to NDR and strong shift is energy, possibly due to bipolar tunneling.

Vibronic progressions: For all layers (2^{nd}, 3^{rd}, 4^{th}, 5^{th}) a vibronic excitation peak is observed. The observed vibrational energies fit quite well to reference values of 150 meV. Additionally, we observe effects of the molecular configuration enhancing the intensity of some vibrational peaks of the molecule e.g. tilted and flat or even within the molecule, i.e., different benzene rings of the molecule.

We have shown that lateral and vertical molecular interactions can lead to a change in coupling between molecule and substrate. The effect of lateral interaction depends on the coupling strength and channel (either the TM's d states or the ligand), and ranges from a complex evolution of states for CuPc to no effect for CoPc. Vertical decoupling becomes efficient from the 3^{rd} molecular layer on, while the 2^{nd} layer appears to be in an intermediate state, sufficiently decoupled to show the gas-phase HOMO-LUMO gap, and vibronic coupling, but not completely to provide a second tunneling barrier .